NJC

PAPER

Cite this: *New J. Chem.*, 2025, **49**, 12940

Received 16th April 2025,
Accepted 25th June 2025

DOI: 10.1039/d5nj01654a

rsc.li/njc

(S)-BINOL-derived chiral picolinate ligand as a platform for new polymer frameworks: a pilot study on the effect of the binaphthyl scaffold *vs.* picolinate†

Humberto A. Rodríguez,[a] Daniel A. Cruz,[a] Juan I. Padrón*[a] and Pablo Lorenzo-Luis*[b]

This work proposes a graphical analysis based on a new chiral picolinate of the **(S)-BINOL** derivative, designated as the reference ligand **L1**. The models establish the influence of temperature on **L1** and identify a new coordination polymer (CP) $[Cu_2(pic)_2(OTf)_2(H_2O)_2(Py)]_n \cdot 2n(Py)$ **1**·2(Py), where [Hpic = pyridine 2-carboxylic acid and pic = picolinate], as the predominant structure through the pathway in dioxane at room temperature or the known complex $[Cu(pic)_2 \cdot 2H_2O]$ **2**·$(H_2O)_2$ at reflux in dioxane. This work provides a detailed description of the preparation method, the structural characteristics of the new CP containing the zinc complex $[Zn_2(pic\text{-}Hpic)_3]_n \cdot n(OTf)$ **3**·(OTf), and density functional theory (DFT) calculations. Coordination polymer **1** 2(Py) exhibits unusual magnetic properties at low temperature and high magnetic fields. This behavior may be associated with the presence of superparamagnetic particles or the influence of crystal field effects. In contrast, its origin is unlikely to be associated with common ferromagnetic impurities such as Fe, Co or Ni due to its characteristic high Curie temperature.

Introduction

Axial chirality is a special case of chirality present in allenes and in biaryl compounds such as 1,1′-binaphthyl-2,2′-diol{(*R*/*S*)-BINOL}, giving rise to chiral atropisomers. Unlike central chirality, the most common form in organic compounds, axial chirality does not require a chiral center. Instead, it arises from a chiral element, specifically a chiral axis (Scheme 1a).[1–7]

The {(±)-BINOL} ligand and its derivatives have been extensively employed and investigated for the synthesis of novel compounds in various fields, including circularly polarized luminescence (CPL), enantiomeric separation, biological transmembrane transport, and asymmetric catalysis.[8]

A more specific case involves its use to develop chiral Brønsted acids, particularly in combination with phosphoric acid to generate BINOL derivatives. In such a case, a chiral pocket containing both the acidic proton and the basic phosphoryl oxygen is created. This structure has been used as a building block together with various metal centers to achieve covalent organic frameworks (COFs).[9] Usually, due to its hindered chiral pockets (Scheme 1b), it binds poorly to M-π-Lewis metals (M^{II} = Fe, Co and Cu). However, it binds well through the phosphoric acid oxygens, alternating two metal atoms with two phosphinate groups in the case of M-π-Lewis metals (M^{II} = Rh, Pd; M^{III} = Yb). In our previous work on a new copper chiral

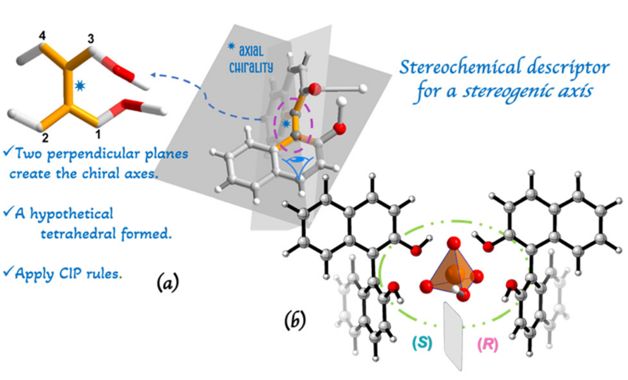

Scheme 1 (a) If a line connecting the highest priority groups 1 → 2 → 3 rotates clockwise, the descriptor to the right is R_a. In contrast, the descriptor for an anti-clockwise rotation is S_a. (b) ((*S*/*R*)-BINOL)-derived chiral phosphoric acid (CPA).

---

[a] *Instituto de Productos Naturales y Agrobiología, Consejo Superior de Investigaciones Científicas (IPNA-CSIC), 38206, La Laguna, Tenerife, Islas Canarias, Spain. E-mail: jipadron@ipna.csic.es*

[b] *Área de Química Inorgánica, Departamento de Química, Universidad de La Laguna, C/Astrofísico Francisco Sánchez 3, 38071 La Laguna, Spain. E-mail: plorenzo@ull.es*

† Electronic supplementary information (ESI) available: A full characterisation of **L1**, **1**·2(Py) and **3**·(OTf). CCDC 2409918, 2409920 and 2409919. For ESI and crystallographic data in CIF or other electronic format see DOI: **https://doi.org/10.1039/d5nj01654a**

polymer (CCP), which exhibited a paddle wheel structure, the difficulty of obtaining other complexes of this metal series (Sc–Zn) was observed.[10] This result prompted us to explore other possibilities while maintaining this type of chiral scaffold containing aromatic rings.[11]

It is important to emphasize that in the design of new ligands, we must consider the reactivity of the metal, the binding modes or the stereoselectivity of the metal complexation. These processes can be affected by steric hindrance, when a molecular fragment blocks the approach of the reagent to the substrate.[3] In addition, there are self-reactivity processes that give rise to aggregates of the ligand in solution and facilitate crystallization mechanisms with the metal present.[12] Although it may seem that a part of the reaction is out of control, this situation allows us to thoroughly explore multiple synthetic conditions while looking for stable complexes.

Various synthetic methodologies for picolinates have been reported in the literature. The chelating features of Hpic have attracted much research attention due to its biological interest. However, to the best of our knowledge, those authors have not provided additional information to support this affirmation.[13–22] Furthermore, no comparative study has explored the influence of {(±)-BINOL} in the chelating behavior of the anionic pic and their role as a ligand.

Herein, we present new insights into the **(S)-BINOL**-derived chiral picolinate as a benchmark **L1** ligand, which allows for two new coordination polymers (CPs) $[Cu_2(pic)_2(OTf)_2(H_2O)_2(Py)]_n\cdot 2n(Py)$ **1**·2(Py) and $[Zn_2(pic\text{-}Hpic)_3]_n\cdot n(OTf)$ **3**·(OTf). Both have κ^{2}N,O groups and are octacoordinated. However, one is unprecedented, exhibiting μ-κ:O′ mode alternating pentacoordinate units (Scheme 3). Complex $[Cu(pic)_2\cdot 2H_2O]$ **2**·$(H_2O)_2$ has been previously reported,[20] and it has been included here for comparative purposes (Scheme 4). The transformation **L1** → **1**·2(Py) suggests that the benchmark ligand **L1** undergoes a process of hydrolysis, followed by a decarboxylation.[23–25] To further verify these transition pathways, different studies were carried out, including density functional theory (DFT) calculations. Finally, the thermal stabilities for the complexes and magnetic properties of **1**·2(Py) are systematically discussed.

Experimental section

Formation and characterization of new ligands

Picolinic acid (**Hpic**) was combined with **(*S*)-BINOL** *via* Steglich-type esterification,[11] providing a new binaphthyl chiral scaffold **L1** (Scheme 2). Even so, we have achieved synthetic conditions that allow for the formation of **L2**, **L3** and **L4** ligands from the starting reagents. A scope of its synthetic process can be found in the ESI.†

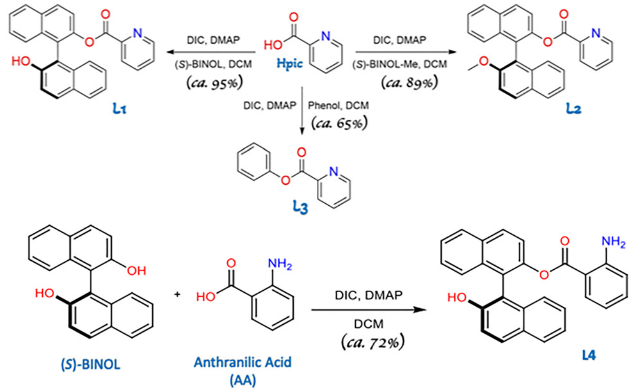

Scheme 2 Straightforward preparation of new binaphthyl chiral scaffolds based on **(S)-BINOL** and/or picolinates.

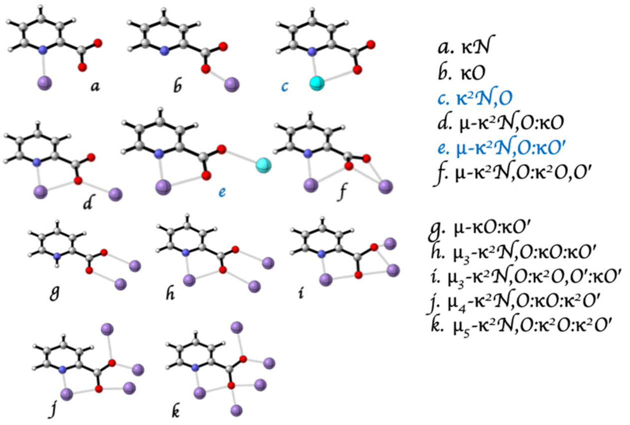

Scheme 3 Coordination modes of Hpic to ion metals: adapted from ref. 16. Modes type c and e are discussed in this work (blue atoms).

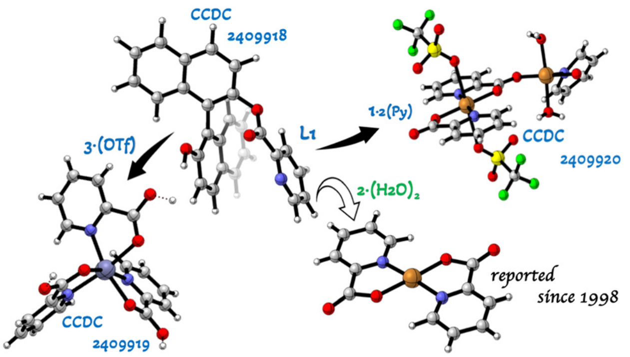

Scheme 4 Benchmark **L1** ligand and its relationship with the findings of the new coordination picolinate **1**·2(Py) and **3**·(OTf) complexes. Complex **2**·$(H_2O)_2$ has been included for comparative purposes.

Results and discussion

Synthesis of the L1 ligand by picolinic acid

L1 was obtained with DCM, and the yield decreased significantly when THF was used. The **Hpic** subunit was chosen based on its accessibility and properties as an achiral product. However, it is also a key design feature because the **Hpic** subunit can exhibit coordination modes as a multidentate ligand (Scheme 3). X-ray quality single crystals of **L1** were obtained (Fig. 1). Full details of this synthetic process, as well as X-ray crystallographic data with the key results, can be found in the ESI.†

Mechanism of the transition pathways and DFT calculations

As shown in Scheme 4, the proposed transition pathways **L1** → **1**·2(Py) and **L1** → **2**·$(H_2O)_2$ are based on experimental results and literature reports.[23–25]

Whereas the first transition pathway requires the presence of water and involves a process of hydrolysis followed by a decarboxylation, the second one does not display any relationships except for the temperature factor. In fact, at room temperature, the yield of **1**·2(Py) is due to the interaction of traces of water molecules absorbed by the dioxane used as solvent.

In contrast, under reflux conditions with dioxane, the reflux temperature favoured the coordination of Cu–N as a traditional dative bond, yielding complex **2**·$(H_2O)_2$.[20] These effects should not be the main reasons for the observed trend. Upon thorough examination of the products of the hydrolysis and decarboxylation, it was found that the binaphthyl framework detaches from the chiral scaffold, enabling the pyridine moiety to separate from the picolinate group and coordinate with the copper ion (Scheme 5, paths I, II). In 2009, Goossen *et al.*[25] reported on a photodecarboxylation reaction with aromatic carboxylic acids, where copper is highly beneficial in the presence of bipyridine ligands or aromatic amines as solvents. We believe that our process is additionally favored by the presence of triflate ions (OTf = $^{-}OSO_2CF_3$) in the solution media. In fact, the access of water molecules to interact with complex units, leading to their dissolution, is known to be less problematic for $^{-}$OTf than, *e.g.*, BF_4^{-} salts.[26] To understand this behavior, an alternative synthesis of **1**·2(Py) was carried out from **2**·$(H_2O)_2$ at room temperature. However, **2**·$(H_2O)_2$ does not revert into complex **1**·2(Py) (Scheme 5, path III).

To the best of our knowledge, no other experimental evidence has been found to support different pathways. In fact, the structure of **1**·2(Py) has been unequivocally confirmed by single-crystal X ray diffraction, confirming the coordination of pyridine, water and $^{-}$OTf moieties to copper instead of the binaphthyl framework (*vide infra*).

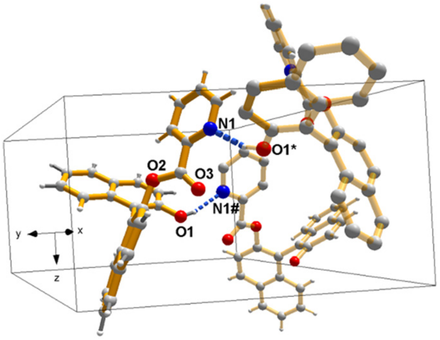

Fig. 1 View of the packing diagram of the benchmark **L1** ligand showing the weak interaction (D–H···A/Å: D···A, H···A):O1–H1···N1$^{\#}$:2.799(6), 1.985(5); {$^{(\#)}$ 1 − *y*, *x* − *y*, 1/3 + *z*; $^{(*)}$ 1 − *x* + *y*, 1 − *x*, −1/3 + *z*}.

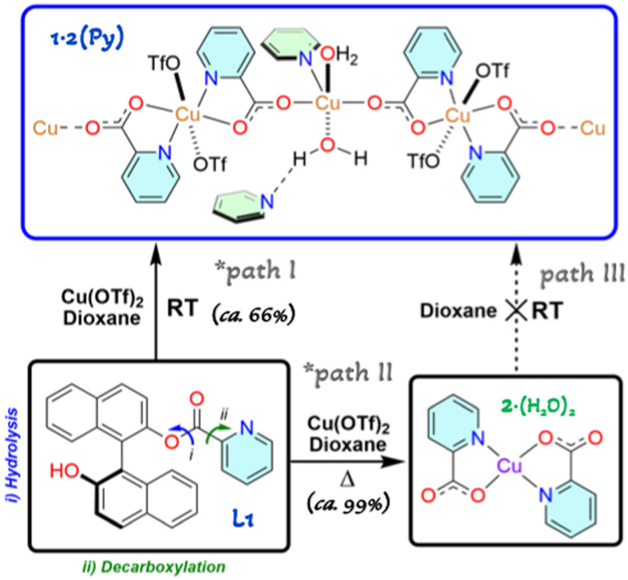

Scheme 5 Proposed pathways **L1** → **1**·2(Py), **L1** → **2**·$(H_2O)_2$, and their relationship with the finding of **1**·(Py). *Dioxane can absorb water from the reaction medium due to its high solubility and miscibility in water: $S(H_2O)^{20\,°C} = 10^3$ g L^{-1}.

In order to address the above questions, $[Zn_2(\text{pic-Hpic})_3]_n\cdot n(OTf)$ **3**·(OTf) was synthesized through **L1**, where $Cu(OTf)_2$ was replaced by $M(OTf)_2$ (M^{II} = Fe, Ni, Zn) in dioxane at room temperature. The composition of **3**·(OTf) was clearly supported by the determination of its crystal structure by single crystal X-ray diffraction (*vide infra*). A scope of this synthetic process with the key results can be found in Scheme 4 and ESI.† Therefore, as we had already anticipated, when iron, nickel or zinc replace copper, the decarboxylation process in water decreases in comparison to hydrolysis. In fact, for iron and nickel, colorless crystals that were suitable for X-ray diffraction were obtained. However, they unfortunately corresponded to **(S)-BINOL**.

Therefore, we conclude that the hydrolysis and decarboxylation pathways should not be viewed as independent processes, but rather as ones that benefit from an effective catalytic partner. It is also worth noting that water is far from an innocent solvent: it can interact with the reactants, products and reaction intermediates.[8,27] In fact, water acts as a nucleophile and as a hydrogen donor for up to two bridges, and also serves as an acceptor of the hydrogen atom in the interaction with other water molecules. We cannot ignore that the acidity of the hydroxyl groups from BINOL show a polarization effect under a natural inductive effect (–I), allowing for the oxonium species H_3O^+. However, this formula is a simplified description of the situation of the H^+ ion in water, where the cation is believed to associate *via* inter-hydrogen bonds with more than one water molecule, giving rise to a complex species of formula $[H(H_2O)_n]^+$. Likewise, the way that aromatic ligands arrange themselves around metal ions can be influenced by the hydrophobic effects caused by water.[28] These intermolecular interactions could provide an additional stabilization with OTf ions,

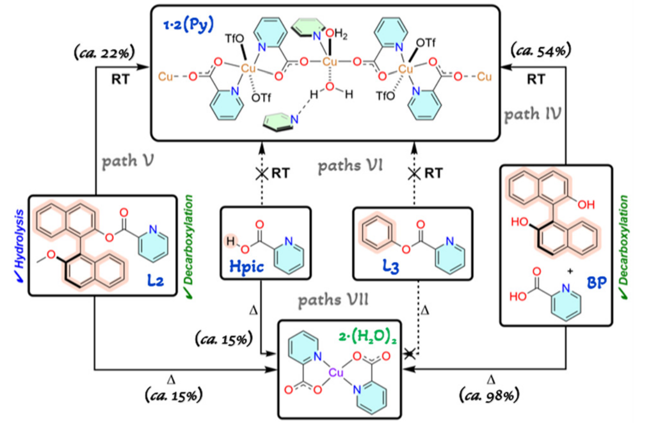

Scheme 6 Proposed pathways **BP** → **1**·(Py) and **L2** → **1**·2(Py), and their relationship with the finding of the picolinate complex **1**·2(Py).

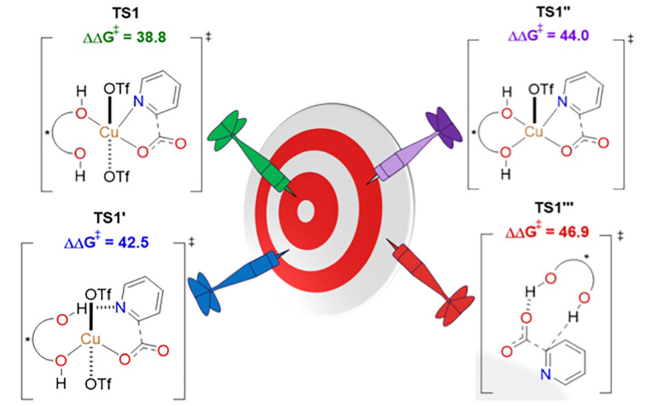

Scheme 7 Possible transition states associated with the decarboxylation process of Hpic (energy values in kcal mol^{-1}). *Indicates the unit of **(S)-BINOL**.

allowing for hydrolysis and the later decarboxylation process. A similar approach was proposed by G. Dunn and H. Thimm,[23] who reported that intramolecular hydrogen bonding is not an important feature of picolinic acid decarboxylation in water. This fact apparently does not contradict our last supposition; although at the moment, everything points towards the important role played by BINOL.

To confirm this hypothesis, **1**·2(Py) and **2**·$(H_2O)_2$ were alternatively synthesized (Scheme 6) from the starting reagents **(S)-BINOL** and Hpic (**BP**), and through ligand **L2** (Scheme 2) under the same experimental conditions described in Scheme 5. As expected, **1**·2(Py) was found with the lowest yield (22%, *via* **L2**). Meanwhile, with **BP**, it showed a significant yield (54%) which was still lower than that for benchmark **L1** ligand (66%, Scheme 5, path I). The progressive decrease in yield for **1**·2(Py) denotes the strong negative effect of non-covalent interactions on the hydrolysis and its later influence under the decarboxylation process. In fact, the attempt to isolate **1**·2(Py) *via* **L3** (Scheme 2) was unsuccessful. In its case, only **2**·$(H_2O)_2$ was obtained *via* **Hpic** with insufficient results (15% yield, Scheme 6, path VII).

It is important to stress that the reaction of **L4** (Scheme 2) and between **Hpic** with phenol (**PP**, ESI†) in dioxane to elucidate the transition pathway did not give rise to the formation of **1**·2(Py). All of our attempts to obtain good quality monocrystals for X-ray diffraction experiments were unsuccessful. The powder diffraction spectra obtained from the final products of both reactions were not consistent with the formation of the **1**·2(Py) complex (Fig. S5 and S6, ESI†).

Additionally, DFT calculations were carried out to gain further insight into the formation process of **1**·2(Py) at the PCM(1,4-dioxane)-ωB97XD/def2-TZVP//PCM(1,4-dioxane)-ωB97XD/def2-SVP level (Scheme 7). Different transition states associated with the decarboxylation of picolinic acid were considered. The most favorable pathway (**TS1**, $\Delta\Delta G^{\ddagger} = 38.8$ kcal mol^{-1}) evolves from an intermediate (INT1) in which the picolinate coordinates in a κ^2N,O mode (Scheme 3), leading to the generation of an arylcuprate. It was observed that copper activates the carbonyl group and subsequently facilitates the cleavage of the C–C bond to generate CO_2. Pyridine is then formed *via* a protonolysis process, as proposed by J. Goossen *et al.*[25] The next closest system (**TS1′**) involves a κ,O coordination mode of the picolinate with copper, being slightly less favored ($\Delta\Delta G^{\ddagger} = 42.5$ kcal mol^{-1}), followed by **TS1″** ($\Delta\Delta G^{\ddagger} = 44.0$ kcal mol^{-1}), where the possibility of losing one triflate unit was considered. Finally, to demonstrate that the presence of copper is essential for the process, **TS1‴** was calculated with $\Delta\Delta G^{\ddagger} = 46.9$ kcal mol^{-1}, a value that is significantly higher than the others. To the best of our knowledge, the decarboxylation process is complex, and a more favorable transition state leading to the formation of the pyridine unit cannot be ruled out. Alternative pathways are currently being explored with new DFT calculations.

Description of the structures of the 1·2(Py) and 3·(OTf) complexes

Complex $[Cu_2(pic)_2(OTf)_2(H_2O)_2(Py)]_n\cdot 2n(Py)$ **1**·2(Py) crystallizes in a tetragonal space group $I41/a$ (Table S4, ESI†). Its molecular structure consists of a polymer, considering the {pic-ligand} and the $[Cu(OTf)_2]$ or $[Cu(H_2O)_2]^{2+}$ units as the two-fold connector and nodes, respectively (Fig. 2). Two interconnected chains are observed, with one oriented along the *a*-axis and the other along the *b*-axis (Fig. S5a, ESI†). The geometry at the Cu1 center exhibits bond lengths along the axial plane that are larger than the bond distances in the equatorial plane: Cu1–O12 2.517(8) Å $[^{(\#)} = -1/4 + x,\ 7/4 - y,\ 3/4 - z]$ *vs.* Cu1–O1 1.964(5), Cu1–N1 1.956(6) Å $[^{(*)} = 1 - x,\ 3/2 - y,\ z]$. This observation may be ascribed to the Jahn–Teller effect. In addition, the metal ion does not deviate from the coordinated plane (Cu1: 0.000 Å), while the values of the stretching ζ and angular Σ are 1.49 Å and 40.1°, respectively. The value of the torsional Θ distortion of the octahedron is found to be 152.7°, which is far from the referenced value for a trigonal prismatic D_{3h} geometry ($\Theta \leq 1170^\circ$).[29] It is possible that the found Θ value comes from the constraints of the picolinate ligand adopting the bidentate κ^2N,O coordination mode,[23] towards Cu1 through the N1 and O1 (bite angle of 83.5(2)°). Alternatively, the Cu2 ion is linked through the O2 bridge adopting the

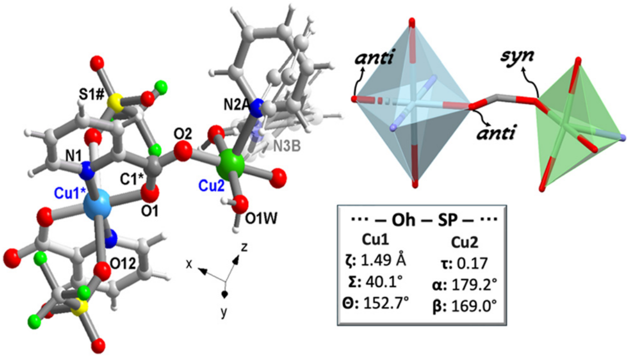

Fig. 2 Molecular structure of **1**·2(Py): the N3A-pyridine solvent molecule has been omitted for clarity (Fig. S5a, ESI†). Schematic of a mostly octahedral structure around Cu1 (OctaDist-program: ζ, Σ, and Θ) and a square-pyramid structure around Cu2 (Addison parameter τ_5).

monodentate μ-κO′ coordination mode described from a square-pyramid geometry environment, according to the Addison parameter tau (τ_5),[30] of 0.17 (Fig. 2). Furthermore, it does not deviate significantly from the coordinated plane (0.006 Å). On the other hand, the value of the separate Cu1···Cu2 ions is larger than the sum of the corresponding vdW radii of two copper atoms (5.00 *vs.* 2.80 Å), with an angle of 67.7(3)° observed between the planes. The carboxylate attached to the Cu1 and Cu2 ions induces a μ-*anti*, *syn*-carboxylate and μ-*syn anti*-carboxylate with the Cu1–O1–C1–O2 and Cu2–O2–C1–O1 torsion angles −173.6(6)° and 1.6(9)°, whereas the bridging pathways Cu1···O2 and Cu2···O1 are 3.939(5) and 3.048(5) Å apart, respectively. The crystal packing diagram shows the intermolecular interactions among the pyridine units as solvent molecules that provide an additional stabilization of the structure. These interaction distances are within the accepted range for intermolecular (D–H···A/Å: D···A, H···A): OW1–H1Wb···N3B: 2.661(2), 1.891(4) hydrogen bonds in coordination complexes (*vide infra*).[10] The distances are comparable to those observed previously for Cu(II) in building coordination polymers (CPs) based on the similar pyridine–carboxylate ligands.[14–20] It should be noted that both modes of coordination observed in **1**·2(Py) form a rare topology in comparison to those reported in the literature, except for that described as Cu(pyridine-2-carboxylate)Cl by B. Zurowska and J. Mrozinski, where each carboxylate ligand acts as the *syn–anti* bridge between two copper ions.[18]

Complex $[Zn_2(\text{pic-Hpic})_3]_n{\cdot}n(\text{OTf})$ **3**·(OTf) crystallizes in the trigonal space group $P\bar{3}$ (Table S6, ESI†), and its crystal unit cell contains a racemic mixture of Λ- and Δ-configured Zn1 centers within the achiral polymeric cationic units $[Zn_2(\text{pic-Hpic})_3]_n^{+}$, with n(OTf) ions acting as solvent molecules for each complex. An intermolecular hydrogen bond O–H···O link in the complex molecule is formed from the hydroxyl moiety (H–O2), but not to the carbonyl oxygen (O1), which interacts with the metal ion: [D–H···A/Å: D···A, H···A]: #O2–H2···O2& 2.459(2), 1.229(1) [(&) = 1 + *x* − *y*, *x*, −*z*] (Fig. 3). A residual electron density near this oxygen atom that is positioned equidistant between both molecules supports this hydrogen-bonding interaction (Fig. S5b, ESI†). Due to donor coordination by the carbonyl group, the structure is displaced toward an octahedral coordination polyhedron around the metal, as the carbonyl oxygen atoms position themselves at axial or equatorial sites, whereas the picolinate nitrogen atom is located at the positions [Zn1–O1 2.134(2), Zn1–N1 2.122(2) Å].

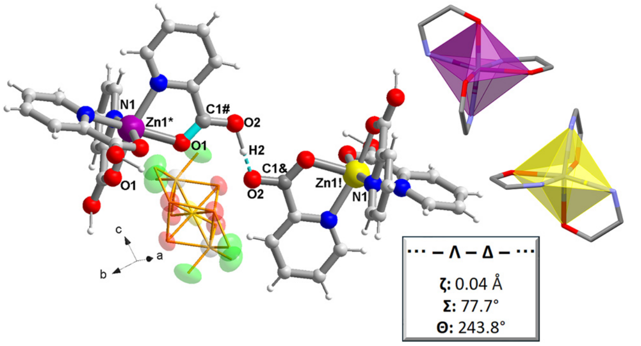

Fig. 3 Molecular structure of **3**·(OTf). Schematic of a mostly octahedral structure around Zn1 (OctaDist-program: ζ, Σ, and Θ).

The Hpic torsion angles Zn1*–O1–C1#–O2 and O2–C1&–O1–Zn1! lie at approximately ±179.5(2)° [(*) = *x*, *y*, 1 + *z*;(!) = 1 − *x*, 1 − *y*, −*z*]. The metal does not deviate significantly from the mean equatorial plane (Zn1: −0.007 Å), while the values of the stretching ζ and angular Σ are 0.04 Å and 77.7°, respectively. Similar to what was observed in **1**·2(Py), the slightly distorted octahedral coordination polyhedron[29] around the metal (Θ = 243.8°) comprises the κ^2N,O coordination mode [bite angle of 77.5(5)°]. The degree of coordination is consistent with earlier work involving nitrogen and oxygen donor action: [Zn(2-H)(2)X], (X = Br, Cl), $[Zn(2\text{-}H)_2(H_2O)_2]$,[22] and $[Zn(C_6H_4NO_2)_2(H_2O)_2]$,[31] showing that the respective donor–acceptor Zn–O and Zn–N bond lengths are comparable to that for **3**·(OTf) (mean values 2.100 and 2.110 Å, respectively). In contrast with that previous reported, **3**·(OTf) is the first structurally characterized example of a zinc(II)-based picolinate complex where the carboxyl hydrogen atom, H2, of one zinc-picolinate molecule is involved *via* hydrogen bonding with one of the hydroxyl oxygen atoms, O2, of an adjacent cinc-picolinate molecule. The carbonyl oxygen atom O1 is involved in donor action with the metal ion. In fact, to our knowledge, a metal–organic framework exhibiting this similar network has been previously reported by W. Ng *et al.*,[32] for an iron picolinate formulated as $[Fe^{II}(C_6H_{4.5}NO_2)_3]^{0.5+}$.

Thermal and magnetism evaluation

It was found that upon careful soft vacuum process of the crystalline sample **1**·2(Py), the complex remained stable under normal temperature and humidity conditions. To confirm the fully anhydrous phase of **1**·2(Py), TG analysis was performed between 70 to 290 °C (Fig. 4, path a). The preliminary results show a first weight loss with two overlapped stages {70–136 °C: *ca.* 21% weight loss, $[\text{DTG}]_{\text{peak}}$ at 130 and 136–290 °C: *ca.* 11% weight loss, a shoulder *ca.* 176 °C}, which are attributable to the loss of pyridine and coordinated water, followed by the likely loss of the ion ⁻OTf. The involvement of this pyridine molecule in an extended hydrogen-bonding network (*vide supra*) can

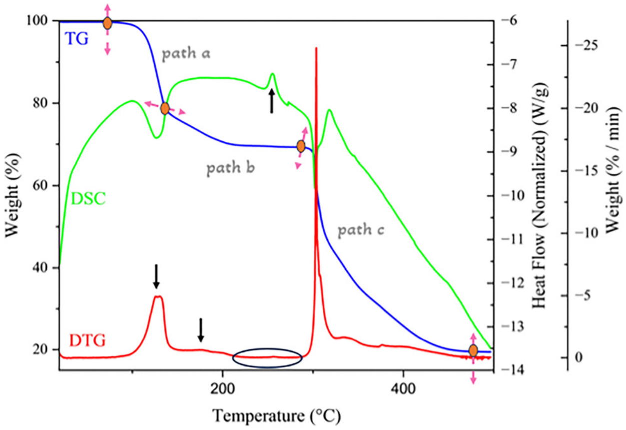

Fig. 4 TG/DTG-DSC curves of **1**·2(Py): network from the overlapped and stability stages (paths (a) and (b)); network from the beginning of the pyrolytic phase (path (c)). TG = mass loss (percent); DTG = percent per minute and DSC = ΔT (microvolts) (↓ exo).

justify this overlapping step. This well-defined thermal process between 70 °C to 290 °C is correlated with the loss of two pyridine molecules, two water molecules and zero point six $^{-}$OTf per formula unit (calcd 32% *vs.* found 36%). It is noteworthy that after this first double overlap step, one short stability of the remaining network is observed up to 290 °C {DTG curve}. The one strong peak that is observed as an endothermic process {[DSC]$_{\text{peak}}$ at 254 °C} corresponds to the coordinated triflate beginning to decompose and converting into stable CuF_2, along with volatile components that were not further analyzed (Fig. 4, path b). This thermal process is well-defined in the literature.[17,33,34] Finally, a strong peak as a mass loss is observed {Fig. 4, path c, [T_{peak}]$_{\text{DTG}}$ = 303 °C}, which is due to the start of a thermolysis process and the remaining CuF_2 compound (Fig. 4, path c). Complex **1**·2(Py) was found to be thermically different, while **3**·(OTf) showed behavior that was similar to **2**·$(H_2O)_2$ (Fig. S2 and S3, ESI†).

Additionally, the magnetic characterization of **1**·2(Py) was performed, revealing a linear dependence of magnetization (M) with respect to the applied field (H) (Fig. S9, ESI†), which is indicative of paramagnetic behaviour. This is observed despite the intrinsic contributions from the diamagnetic components surrounding the Cu^{2+} atoms. M–H measurements at low temperature (1.8 K) showed a trend toward magnetization saturation above 5 T, resulting in a paramagnetic moment close to 2 Bohr magnetons at 7 T. This phenomenon, which is absent at 300 K (Fig. 5), may be associated with superparamagnetic particles or the influence of crystal field effects. While the results are clear, complementary techniques such as EPR spectroscopy or AC susceptibility could be employed to clarify these findings. The effective experimental paramagnetic moment was determined from M *vs.* T measurements at 300 K (Fig. S12, ESI†) using the Curie–Weiss law, yielding a value of $2.06 \pm 0.15\mu_B$ f.u.$^{-1}$ This is lower than the theoretical value ($2.45\mu_B$), which is consistent with the spin-only approximation. Conversely, the paramagnetic Curie–Weiss temperature, obtained from fittings up to 300 K (Θ between +4 and +26 K), shows a value close to 0 K. This is consistent with a predominantly paramagnetic behavior. This magnetic behaviour is well-defined in the literature.[18]

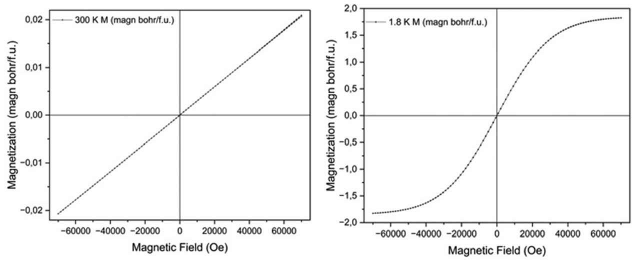

(a) (b)

Fig. 5 Magnetization measurements against the magnetic field, up to 7 Tesla (70 kOe), of **1**·2(Py) at 300 K (a) and at low temperature (1.8 K). (b) Magnetization (magn bohr per f.u.) *vs.* magnetic field (Oe).

Conclusions

Combining picolinic acid (Hpic) with **(S)-BINOL**, a new binaphthyl chiral scaffold **L1** was obtained. One would expect the chiral metal–organic network process to be produced by the link of carbonyl and/or hydroxyl moieties since this process should provide some electron density at the metal ion and strengthen its coordination. However, the straightforward preparation of new chiral **(S)-BINOL**-picolinate derivatives suggests the important role that BINOL plays in obtaining new coordination polymer (CP) picolinic acid derivatives. The experimental results suggest that benchmark **L1** ligand undergoes a hydrolysis process, followed by a decarboxylation pathway. These should not be viewed as independent processes, but rather as ones that benefit from an effective catalytic partner. Its discovery opens the door to the development of another metal–organic assembly, such as the zinc complex **3**·(OTf) obtained for comparative purposes. Whereas the **1**·2(Py) complex requires the presence of water, involving a process of hydrolysis followed by a decarboxylation, the **3**·(OTf) complex does not display this relationship except for the temperature factor.

Author contributions

Humberto A. R., Daniel A. C., Juan I. P., and Pablo L. L. performed, conceived and designed the experiments. All authors contributed equally to writing the manuscript. Humberto A. R. conceived and designed the DFT calculations.

Conflicts of interest

The authors declare no conflict of interest.

Note added after first publication

This version replaces the version originally published on 25th June 2025, in which the captions for Fig. 1 and Scheme 4 were included under the wrong images.

Data availability

The data supporting this article have been included as part of the ESI.†

Acknowledgements

Grant PID2021-126747NB-I00 was funded by MCIN/AEI/10.13039/501100011033 and by "ERDF A way of making Europe". H. A. R. thanks the Spanish MCIU for an FPU scholarship. We thank the SQUID Magnetometry and Low Temperature service of the ICMM-Madrid for the magnetic characterization. We also acknowledge the use of the SEGAI-ULL service for IR, X-ray and thermal analysis.

References

1 N. Mukherjee, B. Mondal, T. N. Saha and R. Maity, Palladium, iridium, and rhodium complexes bearing chiral N-heterocyclic carbene ligands applied in asymmetric catalysis, *Appl. Organomet. Chem.*, 2024, **38**, e6794.
2 X.-F. Bai, Y.-M. Cui, J. Cao and L.-W. Xu, Atropisomers with Axial and Point Chirality: Synthesis and Applications, *Acc. Chem. Res.*, 2022, **55**, 2545–2561.
3 M. Mancinelli, G. Bencivenni, D. Pecorari and A. Mazzanti, *Eur. J. Org. Chem.*, 2020, 4070–4086.
4 P. Ll.-Williams and E. Giralt, Stereogenic Centers and Axes: A Comparison of the Chiral Topologies Available to Cabcd and abC = C = Ccd, *J. Chem. Educ.*, 2005, **82**(7), 1031.
5 J. M. Brunel, BINOL: A Versatile Chiral Reagent, *Chem. Rev.*, 2005, **105**, 857–897.
6 R. Kshatriya, Recent Advancement in H8–BINOL Catalyzed Asymmetric Methodologies, *ACS Omega*, 2023, **8**, 17381–17406.
7 E. M. da Silva, H. D. A. Vidal, M. A. P. Januário and A. G. Corrêa, Advances in the Asymmetric Synthesis of BINOL Derivatives, *Molecules*, 2023, **28**(1), 12.
8 Y. Yu, Y. Hu, C. Ning, W. Shi, A. Yang, Y. Zhao, Z.-Y. Cao, Y. Xu and P. Du, BINOL-Based Chiral Macrocycles and Cage, *Angew. Chem., Int. Ed.*, 2024, **63**, e202407034.
9 X. Wu, X. Han, Q. Xu, Y. Liu, C. Yuan, S. Yang, Y. Liu, J. Jiang and Y. Cui, Chiral BINOL-Based Covalent Organic Frameworks for Enantioselective Sensing, *J. Am. Chem. Soc.*, 2019, **141**, 7081–7089.
10 H. A. Rodríguez, D. A. Cruz, V. Lavín, J. I. Padrón and P. Lorenzo-Luis, Novel dinuclear open paddle-wheel-like copper complexes involving π-stacking on the basis of chiral binaphthyl phosphoric acid {(R)-PhosH}: structural, magnetic and optical properties, *Dalton Trans.*, 2024, **53**, 18099.
11 A. Jordan, K. D. Whymark, J. Sydenham and H. F. Sneddon, A solvent-reagent selection guide for Steglichtype esterification of carboxylic acids, *Green Chem.*, 2021, **23**, 6405.
12 Y.-D. Peng, F. Huang, M.-X. Du, Y.-T. La, J. Yu, X. Hu and W.-K. Dong, Rare formyl-coordinated homotrinuclear copper(II) salamo-based N_2O_3-donor complex: Experimental and theoretical studies, *Inorg. Chim. Acta*, 2024, **560**, 121815.
13 R. S. Grant, S. E. Coggan and G. A. Smythe, The Physiological Action of Picolinic Acid in the Human Brain, *Int. J. Tryptophan Res.*, 2009, **2**, 71–79.
14 Ö. Tamer, D. Avcı and Y. Atalay, A novel Cu(II) Complex of Picolinate and 1,10-Phenanthroline: Preparation, Crystal Structure Determination, Spectroscopic Characterization and Nonlinear Optical Studies, *J. Inorg. Organomet. Polym.*, 2017, **27**, 700–713.
15 L. C. Orjiekwe, F. A. S. Fabiyi and D. A. O. Edward, Synthesis and characterization of new picolinate metal complexes, *Synth. React. Inorg. Met.-Org. Chem.*, 2007, **35**(9), 695–702.
16 D. Huang, W. Wang, X. Zhang, C. Chen, F. Chen, Q. Liu, D. Liao, L. Li and L. Sun, Synthesis, Structural Characterizations and Magnetic Properties of a Series of Mono-, Di- and Polynuclear Manganese Pyridinecarboxylate Compounds, *Eur. J. Inorg. Chem.*, 2004, 1454–1464.
17 Z. Herena, C. Kesera, C. C. Ersanlı, O. Z. Yesilelc and N. Ocak, Synthesis, Spectral and Thermal Studies, and Crystal Structure of *cis*-Bis(4-methylimidazole)bis(picolinato)copper(II)[Cu(pic)2(4-MeIm)2], *Z. Naturforsch., B: J. Chem. Sci.*, 2006, **61**(10), 1217–1221.
18 B. Zurowska and J. Mrozinski, Ferromagnetic exchange coupling in a two-dimensional copper(II) compound: Cu(pyridine-2-carboxylate)Cl, *Inorg. Chim. Acta*, 2003, **342**, 23–28.
19 F. A. Mautner and S. S. Massoud, Structure determination of picolinato–copper(II)-amine complexes, *J. Mol. Struct.*, 2007, **871**, 108–113.
20 P. Seglà, M. Jamnicky, M. Koman, J. Sima and T. Glowiak, Metal(II)-promoted hydrolysis of pyridine-2-carbonitrile to pyridine-2-carboxylic acid. The structure of [Cu(pyridine-2-carboxylate)$_2$]·2H$_2$O, *Polyhedron*, 1998, **17**(25,26), 4525–4533.
21 N. Yasumatsu, Y. Yoshikawa, Y. Adachi and H. Sakurai, Antidiabetic copper(II)-picolinate: Impact of the first transition metal in the metallopicolinate complexes, *Bioorg. Med. Chem.*, 2007, **15**, 4917–4922.
22 S. Enthaler, X.-F. Wub, M. Weidauer, E. Irran and P. Döhlert, Exploring the coordination chemistry of 2-picolinic acid to zinc and application of the complexes in catalytic oxidation chemistry, *Inorg. Chem. Commun.*, 2014, **46**, 320–323.
23 G. E. Dunn and H. F. Thimm, Kinetics and mechanism of decarboxylation of some pyridinecarboxylic acids in aqueous solution. II, *Can. J. Chem.*, 1997, **55**, 1342–1347.
24 M. R. F. Ashwortrh, P. Daffernan and D. Ll, Hammick, The Mechanism of Decarboxylation. Part II. The Production of Cyanide-like Ions from a -Picolinic, Quinaldinic, and iso Quinaldinic Acids, *J. Chem. Soc.*, 1939, 809–812.
25 L. J. Goossen, F. Manjolinho, B. A. Khan and N. Rodríguez, Microwave-Assisted Cu-Catalyzed Protodecarboxylation of Aromatic Carboxylic Acids, *J. Org. Chem.*, 2009, **74**, 2620–2623.
26 A. Jordan, K. D. Whymark, J. Sydenham and H. F. Sneddon, A solvent-reagent selection guide for Steglichtype esterification of carboxylic acids, *Green Chem.*, 2021, **23**, 6405.
27 M. Serrano-Ruiz, P. Lorenzo-Luis and A. Romerosa, Easy synthesis and water solubility of ruthenium complexes

containing PPh_3, mTPPMS, PTA and mPTA, (mTPPMS = meta triphenyphosphine monosulfonate, PTA = 1,3,5-triaza-7-phosphaadamantane, mPTA = N-methyl-1,3,5-triaza-7-phosphaadamantane), *Inorg. Chim. Acta*, 2017, **455**, 528–534.

28 J. E. Conde-González, P. Lorenzo-Luis, V. Salvado, J. Havel and E. M. Peña-Méndez, A new cotton functionalized with iron(III) trimer-like metal framework as an effective strategy for the adsorption of triarylmethane dye: An insight into the dye adsorption processes, *Heliyon*, 2021, e08524.

29 E. G. Percástegui, T. K. Ronson and J. R. Nitschke, Design and Applications of Water-Soluble Coordination Cages, *Chem. Rev.*, 2020, **120**, 13480–13544.

30 R. Ketkaew, Y. Tantirungrotechai, P. Harding, G. Chastanet, P. Guionneau, M. Marchivie and D. J. Harding, OctaDist: a tool for calculating distortion parameters in spin crossover and coordination complexes, *Dalton Trans.*, 2021, **50**, 1086.

31 A. G. Blackman, E. B. Schenk, R. E. Jelley, E. H. Krensked and L. R. Gahan, Five-coordinate transition metal complexes and the value of τ_5: observations and caveats, *Dalton Trans.*, 2020, **49**, 14798.

32 L. Croitor, D. Chisca, E. B. Coropceanu and M. S. Fonari, Diaquabis(pyridine-2-carboxylato κ^2N,O)zinc dimethylformamide hemisolvate, *Acta Cryst.*, 2013, **E69**, m454.

33 D. Onggo, F. Martak, Ismunandar, B. M. Yamin and S. W. Ng, Hemi{tris(picolinic acid- κ^2N,O)iron(II)/tris(picolinato κ^2N,O)iron(II)}hemi(tetrafluoroborate), *Acta Cryst.*, 2006, **E62**, m1112–m1113.

34 F. Cecconi, C. A. Ghilardi, P. Gili, S. Midollini, P. A. Lorenzo Luis, A. D. Lozano-Gorrín and A. Orlandini, Complexation of nickel(II) and lead(II) cations with the tripodal nitrilo-tris(methylene-phenylphosphinic) acid (H3L). X-ray crystal structure of the dimer [Ni(HL)(DMSO)]2·2DMSO, *Inorg. Chim. Acta*, 2001, **319**, 67–74.